Selective single- and double-mode quantum-limited amplifier

Abdul Mohamed,[1] Elham Zohari,[1,2] Jarryd J. Pla,[3] Paul E. Barclay,[1] and Shabir Barzanjeh[1,*]

[1] *Department of Physics and Astronomy, University of Calgary, Calgary, Alberta T2N 1N4, Canada*

[2] *Department of Physics, University of Alberta, Edmonton, Alberta T6G 2E1, Canada*

[3] *School of Electrical Engineering and Telecommunications, UNSW Sydney, Sydney, New South Wales 2052, Australia*

(Received 26 November 2023; revised 4 March 2024; accepted 29 May 2024; published 24 June 2024)

A quantum-limited amplifier enables the amplification of weak signals while introducing minimal noise dictated by the principles of quantum mechanics. Such amplifiers serve a broad spectrum of applications in quantum computing, including fast and accurate readout of superconducting qubits and spins, as well as various uses in quantum sensing and metrology. Parametric amplification, primarily developed with use of Josephson junctions, has evolved into the leading technology for highly effective microwave measurements within quantum circuits. Despite their significant contributions, these amplifiers face fundamental limitations, such as their inability to handle high powers, their sensitivity to parasitic magnetic fields, and particularly their limitation to operate only at millikelvin temperatures. To tackle these challenges, here we experimentally develop a novel quantum-limited amplifier based on superconducting kinetic inductance and present an extensive theoretical model to describe this nonlinear coupled-mode system. Our device surpasses the conventional constraints associated with Josephson-junction amplifiers by operating at much higher temperatures up to 4.5 K. With two distinct spectral modes and tunability through bias current, this amplifier can operate selectively in both the single-mode-amplification regime and the double-mode-amplification regime near the quantum noise limit. Using a nonlinear thin film exhibiting kinetic inductance, our device attains gain exceeding 50 dB in a single-mode configuration and 32 dB in a double-mode configuration, while adding 0.82 input-referred noise quanta. Importantly, this amplifier eliminates the need for Josephson junctions, resulting in the capability to handle significantly higher powers than Josephson junction–based amplifiers. It also demonstrates resilience in the presence of magnetic fields, offers a straightforward design, and increases reliability. This positions the amplifier as a versatile solution for quantum applications and facilitates its integration into future superconducting quantum computers.

DOI: 10.1103/PhysRevApplied.21.064052

I. INTRODUCTION

Parametric amplifiers with noise characteristics at the quantum limit play a central role in quantum processors [1,2], offering significant applications across various quantum systems [3,4]. In the microwave frequency range [3,5–9] these amplifiers enable precise, fast, and high-fidelity single-shot measurements of superconducting qubits [10–13], ensembles of spins [14], quantum dots [15,16], and nanomechanical resonators [17]. Furthermore, the use of near-quantum-limited amplifiers has created new experimental avenues for producing nonclassical radiation, including single- and double-mode vacuum squeezing [18–20] with applications in weak measurement [21,22], axion-dark-matter detection [23–26], and quantum illumination and radar [27–30].

The most-common method for building microwave parametric amplifiers involves superconducting Josephson junctions, configured as a Josephson parametric amplifier (JPA) [31,32] or Josephson traveling-wave parametric amplifier (JTWPA) [3,8,9]. These systems exploit the nonlinear characteristics of Josephson junctions to attain significant amplification with minimal noise. Through precise control facilitated by an external microwave pump, JPAs allow fine-tuning of gain, enabling accurate and efficient amplification of weak signals. Their tunability and instantaneous bandwidth make quantum-limited amplifiers essential tools for advancing quantum information processing and pushing the boundaries of quantum technologies.

Despite their many valuable applications, both JPAs and JTWPAs encounter significant limitations that restrict their

*Contact author: shabir.barzanjeh@ucalgary.ca

effective integration into scalable quantum architectures. Both JPAs and JTWPAs have a limited saturation input power, primarily attributed to the presence of higher-order nonlinearity such as the Kerr nonlinearity. This limitation typically confines them to operate with only a few microwave photons per bandwidth [5,33] and thus limits their ability to effectively handle a wide range of frequencies and higher-power signals. Moreover, Josephson junction–based amplifiers are highly sensitive to parasitic magnetic fields, which can negatively impact their performance. To mitigate this sensitivity, magnetic field isolation is often necessary. Furthermore, they typically require operation at temperatures below 1 K [3,5,9], which can pose practical challenges in applications where higher-temperature operation is desired [27–29].

An alternative approach to overcome these limitations involves the building of quantum-limited amplifiers without the reliance on Josephson junctions by use of superconducting films that possess kinetic inductance. This approach uses a simplified single-step lithography process and uses thin films of high-temperature kinetic inductance superconductors, such as niobium titanium nitride (Nb-Ti-N) [34–40]. The intrinsic kinetic inductance of the Nb-Ti-N film introduces the necessary nonlinearity for achieving quantum-limited amplification, thereby eliminating the need to use Josephson junctions. These amplifiers typically use three-wave-mixing (3WM) [37–40] or four-wave-mixing [41,42] processes to amplify the input signal. The amplification can happen through degenerate or nondegenerate parametric amplification [1,2]. In the case of degenerate or phase-preserving amplification, the idler and the signal have identical frequencies. This configuration offers the potential for noiseless amplification and the generation of single-mode vacuum squeezing [19,43]. In contrast, in nondegenerate or phase-insensitive amplification, the idler and the signal exist as separate modes with distinct frequencies. Within this regime, the amplifier's output can be a two-mode squeezed state or an entangled state [2,44,45]. Resonance-based kinetic inductance amplifiers primarily operate in the single-mode configuration, functioning within degenerate-amplification or near-nondegenerate-amplification regimes [39]. In these configurations, shifting of the pump frequency from twice the resonance frequency effectively initiates a 3WM process, wherein a pump photon is down-converted to idler and signal photons within the resonator mode. However, this approach encounters limitations, particularly when there is a requirement for generating two-mode squeezing and entanglement. This is primarily because the idler and the signal do not represent two spectrally separated modes. Consequently, the development of a quantum-limited amplifier that is tunable, is of low noise, is compatible with high temperatures, and possesses the ability to selectively operate in both the single-mode regime and the two-mode regime remains an outstanding challenge.

In this work, we introduce a quantum-limited kinetic inductance parametric amplifier (KIPA) that overcomes some of the technical limitations associated with Josephson-junction amplifiers and is capable of operating at higher temperatures due to the high critical temperature of the kinetic inductance thin film [46]. The presence of two spectrally and spatially distinct modes, along with the ability to tune the resonance frequency by application of bias current, enables the KIPA to operate selectively in both the single-mode-amplification regime and the dual-mode-amplification regime.

By using a uniformly evaporated thin film of Nb-Ti-N on high-resistivity intrinsic silicon, we achieve exceptional amplification, surpassing 50-dB gain in the single-mode configuration and 32-dB gain in the double-mode configuration, with a gain-bandwidth product of approximately 30 MHz for operation in the 3WM regime. Importantly, our design eliminates the reliance on Josephson junctions, resulting in a significantly higher 1-dB compression point for the output power when compared with amplifiers based on Josephson junction technology [47]. The junction-free design of the KIPA also allows a high degree of resilience to stray magnetic fields or adaptability to experiments requiring strong magnetic fields, reaching up to 2 T [41,42,48,49]. Additionally, compared with the design of other kinetic inductance amplifiers [39], the design of our KIPA is inherently simple and does not require complex circuitry or filtering to generate amplification. The use of kinetic inductance for amplification simplifies the design and fabrication processes to a remarkable degree compared with Josephson junction–based amplifiers. Moreover, it increases reliability since the nonlinearity of our device is an inherent feature of its geometry, eliminating the need for complicated and delicate fabrication procedures. Additionally, we introduce a theoretical model that describes the dynamics of the system and use it to fit the experimental results. We note that while the use of coupled resonators for amplification has been investigated before, previous studies typically focused on configurations where either both resonators contain nonlinearity or where both resonators share a nonlinear medium [50–52]. In contrast, our approach here entails coupling a linear resonator to a nonlinear resonator and harnessing 3WM for amplification in the coupled system.

This paper is organized as follows: In Sec. II, we establish a comprehensive theoretical model to elucidate single-mode and double-mode amplification based on a coupled-mode system. Section III introduces the experimental setup and the KIPA design. Section IV presents the experimental results of single-mode and double-mode amplification. In Sec. V, we discuss the noise properties of the KIPA and study the operation of the device at different device temperatures. Finally, the concluding remarks and discussion are presented in Sec. VI.

II. THEORETICAL MODELING OF AMPLIFICATION

In this section, we provide an in-depth theoretical model that describes the 3WM process and amplification within a generic two-mode coupled system. In the subsequent sections, we divide our discussion into single-mode and double-mode amplification, and we construct separate comprehensive theoretical models for each of these regimes.

A. Hamiltonian

The system under consideration includes a coupled system that incorporates nonlinearity in one of the modes, as shown in Fig. 1. The Hamiltonian describing this coupled-mode system, accounting for parametric processes and operating in the presence of a pump with frequency ω_p and an annihilation operator a_p, can be written as (with $\hbar = 1$)

$$H = \omega_a a^\dagger a + \omega_b b^\dagger b + \omega_p a_p^\dagger a_p + J(a^\dagger b + b^\dagger a) + H_{\text{non}}. \tag{1}$$

where a and b are the annihilation operators of each mode with frequencies ω_a and ω_b, respectively, and with coherent-mode-coupling strength J. We also define the nonlinear Hamiltonian [39,53]

$$H_{\text{non}} = \frac{g_0}{2}(a^2 a_p^\dagger + a^{\dagger 2} a_p) + K a^{\dagger 2} a^2, \tag{2}$$

where the second term in this Hamiltonian describes the degenerate parametric interaction with strength g_0 and the third term represents a four-wave-mixing interaction with strength K. In this Hamiltonian, the inclusion of nonlinearity in one of the modes results in an interesting scenario where we can operate the device in either the single-mode-amplification regime or the double-mode-amplification regime. This choice can be made by our tuning the resonance frequency of mode a, either far from or close to the anticrossing point, where efficient exchange of energy between the two modes occurs. We also note that for our KIPA in the presence of a strong bias current, $K \ll g_0$, and therefore the four-wave-mixing process can be ignored. With a film thickness of 10 nm and a resonator of width 2 μm, the estimated Kerr nonlinearity K will be approximately 1 mHz. As we will see later, this value is a few orders of magnitude smaller for the auxiliary resonator b.

B. Single-mode amplification

Away from the anticrossing point, where the frequency of mode a is well separated from the frequency of the auxiliary mode b, the interaction between these modes does not facilitate photon hopping or exchange of the excitation. Consequently, mode b does not undergo amplification when $|\omega_a - \omega_b| \gg 2J$. In this case, we can treat the system as a single mode, characterized by substantial nonlinearity in mode a; see Fig. 1(a). Therefore, the Hamiltonian of the system in the strong-pump regime is given by [54]

$$H = \Delta a^\dagger a + \frac{g}{2}(a^2 e^{-i\phi_p} + a^{\dagger 2} e^{i\phi_p}), \tag{3}$$

where $g = g_0|\alpha_p|$, in which $|\alpha_p|$ is the amplitude of the pump, and ϕ_p is the global phase set by the pump. The above Hamiltonian has been written in a reference frame rotating at $\omega_p/2 = \omega_a - \Delta$.

The system's output can be written with respect to the input quantum noise (a_{e} with extrinsic damping rate κ_{e}) and the intrinsic losses in the resonator mode (expressed as a_{i} with intrinsic damping rate κ_{i}). Solving the quantum Langevin equations allows us to obtain the output field of the resonator [54]

$$\begin{aligned} a_{\text{out}}(\omega) = &\left[\mathcal{G}_S(\omega) a_{\text{e}} + \mathcal{G}_I(\omega) a_{\text{e}}^\dagger\right] \\ &+ \sqrt{\frac{1-\eta}{\eta}}\left[(\mathcal{G}_S(\omega)+1) a_{\text{i}} + \mathcal{G}_I(\omega) a_{\text{i}}^\dagger\right], \end{aligned} \tag{4}$$

where $\eta = \kappa_{\text{e}}/\kappa$ describes the waveguide-resonator coupling, with $\kappa = \kappa_{\text{e}} + \kappa_{\text{i}}$, and we define

$$\begin{aligned} \mathcal{G}_S(\omega) &= \frac{\eta\kappa\left[\frac{\kappa}{2} - i(\omega + \Delta)\right]}{\Delta^2 - g^2 + (i\omega - \frac{\kappa}{2})^2} - 1, \\ \mathcal{G}_I(\omega) &= \frac{-i\eta\kappa g e^{i\phi}}{\Delta^2 - g^2 + (i\omega - \frac{\kappa}{2})^2}. \end{aligned} \tag{5}$$

Note that $|\mathcal{G}_I(\omega)|^2 = |\mathcal{G}_S(\omega)|^2 - 1$ for $\eta \approx 1$. The first two terms in Eq. (4) show the amplification of the signal $a_S \equiv a_{\text{e}}$ and idler $a_I \equiv a_{\text{e}}^\dagger$ modes, while the last two terms represent the noise terms added by the KIPA due to the intrinsic loss of the resonator. In the absence of internal loss, $\eta \to 1$, Eq. (4) simplifies to $a_{\text{out}}(\omega) = \sqrt{G} a_{\text{e}} + \sqrt{G-1} a_{\text{e}}^\dagger$, describing the annihilation operator of a degenerate (phase-sensitive) parametric amplifier with gain

$$G = |\mathcal{G}_S|^2 = \left(\frac{2}{1 - 4(g/\kappa)^2} - 1\right)^2, \tag{6}$$

where, for simplicity, we consider $\Delta = \omega = 0$. We can see that for $g \ll \kappa$, the gain is negligible, $G \to 1$. However, the highest gain is achieved near the denominator's roots and as $g \to \kappa/2$, which results in $G \to \infty$. This divergence can be understood better by looking at the stability condition of the system through the susceptibility of the resonator [55]. For $\Delta = 0$, the resonator's susceptibility is

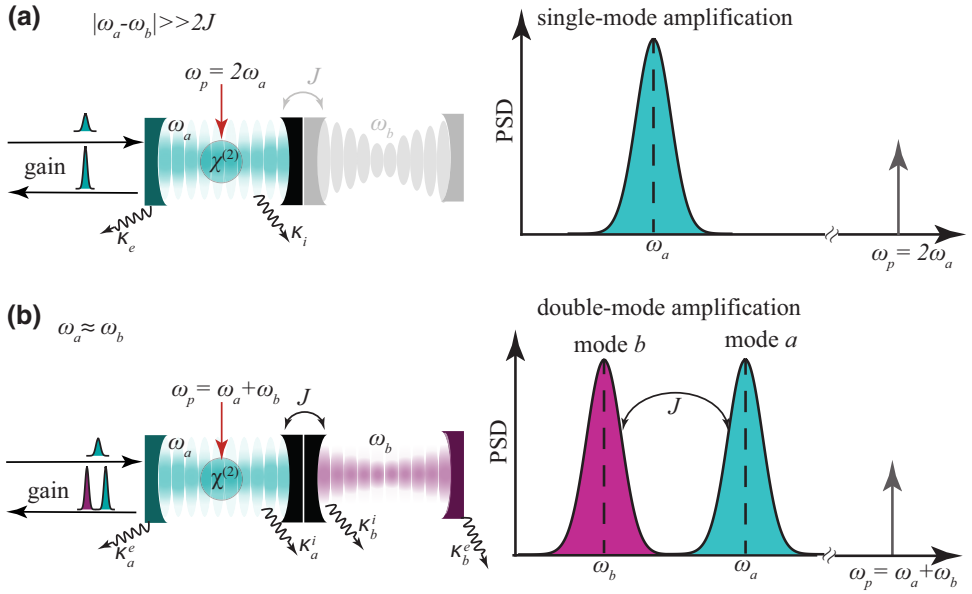

FIG. 1. Schematic representation of a coupled-resonator system exhibiting coupling rate J. Here one resonator, with resonance frequency ω_a and annihilation operator a, is coupled to an auxiliary resonator having resonance frequency ω_b and annihilation operator b. Incorporating a nonlinear medium characterized by a $\chi^{(2)}$ nonlinearity, resonator a facilitates amplification via the 3WM process. The system's operation mode, whether single-mode or double-mode amplification, can be selected by one properly pumping the system. (a) The single-mode-amplification scenario, characterized by a significant separation in resonance frequencies between the two resonators, expressed as $|\omega_a - \omega_b| \gg 2J$. In this setup, the system can be effectively treated as a single mode by one disregarding the dynamics of the auxiliary resonator b. Amplification of the single mode is achieved by application of a strong pump at $\omega_p = 2\omega_a$, resulting in a degenerate amplification in mode a, as seen in the power spectral density (PSD) of the output field. (b) In contrast, by adjustment of the resonance frequencies of the two modes so that they are equal, i.e., $\omega_a = \omega_b$, and by the pumping of the system at $\omega_p = \omega_a + \omega_b$, double-mode amplification is realized, with the two modes being spectrally separated by the coupling rate J. Here $\kappa_j^{e(i)}$ is the extrinsic (intrinsic) damping rate of each resonator $j = a, b$.

given by [54]

$$\boldsymbol{\chi}(\omega) = \frac{1}{\left(i\omega - \frac{\kappa}{2}\right)^2 - g^2} \begin{bmatrix} -i\omega + \frac{\kappa}{2} & -ige^{i\phi_p} \\ ige^{-i\phi_p} & -i\omega + \frac{\kappa}{2} \end{bmatrix}. \quad (7)$$

The stability of the system is determined by the denominator of $\boldsymbol{\chi}(0)$, imposing $g < \kappa/2$ as the stability criterion [2]. This condition ensures that the parametric amplifier operates below its threshold and avoids it entering self-sustained oscillations. However, when $g \geq \kappa/2$, the system becomes unstable and this leads to parametric self-oscillations.

C. Double-mode amplification

The result in Eq. (4) can be extended to nondegenerate, phase-insensitive amplification, where we deal with two spectrally distinct signal and idler modes. This can be achieved by one bringing mode a on resonance with mode b; see Fig. 1(b). The coherent interaction between the two modes, when combined with the 3WM process in mode a, enables the nondegenerate amplification within the coupled system. This becomes evident when we diagonalize the interaction Hamiltonian and write Eq. (1) in the hybridized-mode (collective-mode) representation $c_\pm = a \pm b/\sqrt{2}$:

$$H = \sum_{i=\pm} \omega_\pm c_i^\dagger c_i + \omega_p a_p^\dagger a_p + \frac{g_0}{2}\left[c_+ c_- a_p^\dagger + \text{H.c.}\right] + \frac{g_0}{4}\left[\left(c_+^2 + c_-^2\right) a_p^\dagger + \text{H.c.}\right], \quad (8)$$

where $\omega_\pm = [(\omega_a + \omega_b)/2] \pm \sqrt{(\Delta_{ab}^2/4) + J^2}$ are the frequencies of the collective modes and $\Delta_{ab} = (\omega_a - \omega_b)/2$. In the strong-pump regime and a reference frame rotating at $\omega_p/2 = \Omega - \Delta$, the Hamiltonian (8) reduces to

$$H = \Delta_+ c_+^\dagger c_+ + \Delta_- c_-^\dagger c_- + \frac{g}{2}\left[e^{-i\phi_p}\left(c_+^2 + c_-^2\right) + \text{H.c.}\right] + g\left[e^{-i\phi_p} c_+ c_- + \text{H.c.}\right], \quad (9)$$

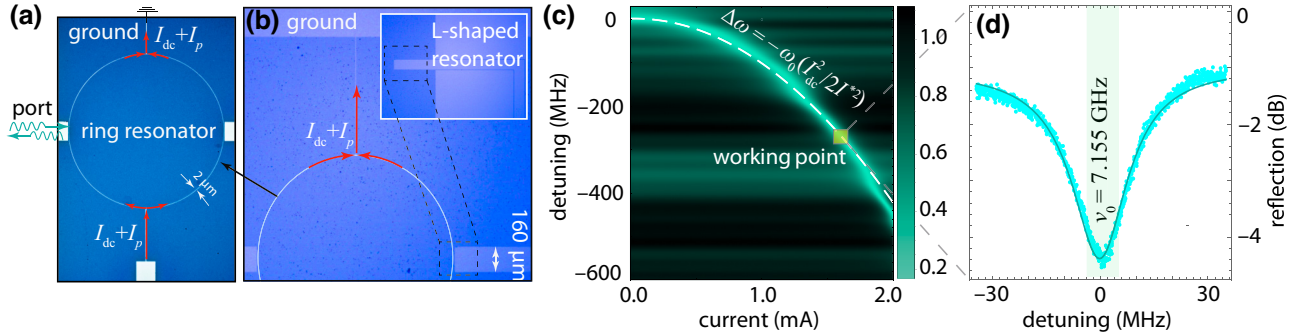

FIG. 2. (a) A ring resonator with a 1.3-mm diameter and a 2-μm pitch is connected capacitively to an auxiliary resonator. The system is probed through a transmission line connected capacitively to the left side of the ring. A separate line provides the pump and direct current from the device's bottom, flowing through the ring. (b) Optical image of the KIPA involving a ring and L-shaped auxiliary resonators. The inset in (b) displays the L-shaped auxiliary resonator with a width of 160 μm and a length of 4 mm. The design prohibits direct current from passing this resonator, effectively setting the 3WM nonlinearity to zero for the auxiliary resonator. (c) Resonance frequency of the ring resonator as a function of applied bias current. The resonance frequency shows a quadratic pattern with respect to the applied current $\Delta\omega = -(\omega_0/2)\,(I_{dc}/I^*)^2$. (d) Resonance frequency of the resonator at fixed current $I_{dc} = 1.575$ mA, corresponding to $\omega_0/2\pi = 7.155$ GHz.

where $g = g_0|\alpha_p|$ and we consider $\Omega \equiv \omega_a = \omega_b$. Note that the third term in this Hamiltonian describes the degenerate amplification in the collective modes, while the last term represents the nondegenerate amplification. The presence of the terms $\Delta_\pm = \Delta \pm J$ in the first two parts of the Hamiltonian enables us to effectively select (activate) degenerate or nondegenerate amplification, given that $2J$ exceeds the total damping rates of the modes $\kappa_\pm$ and the coupling rate g. This condition becomes evident when we move to the interaction picture with respect to $\Delta_+ c_+^\dagger c_+ + \Delta_- c_-^\dagger c_-$,

$$H_{\rm int} = \frac{g}{2}\left[e^{-i\phi_p}\left(c_+^2 e^{-2i\Delta_+ t} + c_-^2 e^{-2i\Delta_- t}\right) + \text{H.c.}\right] + g\left[e^{-i\phi_p} c_+ c_- e^{-2i\Delta t} + \text{H.c.}\right]. \tag{10}$$

By choosing $\Delta = J$ and under the rotating-wave approximation, we effectively disregard the rapidly oscillating terms rotating at a frequency of $2J$. This choice enables us to specifically select degenerate amplification in mode c_-, while $\Delta = -J$ results in amplification in mode c_+. In these situations, the gain in the degenerate parametric amplification can still be described by Eqs. (4) and (5) by our replacing $a_{e/i}$ by $c_\pm^{e/i}$, where $c_\pm^{e/i}$ are the effective noise operators of the hybridized modes, κ by $\kappa_\pm$, Δ by $\Delta_\pm$, and η by $\eta_\pm$. On the other hand, if we choose $\Delta = 0$, which corresponds to $\omega_p = \omega_a + \omega_b$, we can activate nondegenerate amplification or select the terms involving $c_+ c_-$ in the Hamiltonian. In this situation, the contributions of single-mode-amplification terms proportional to $c_\pm^2 e^{\mp 2iJ} + \text{H.c.}$ are negligible under the rotating-wave approximation. By solving the quantum Langevin equation, we can extract the output field for the hybridized modes

$$c_{\pm,\rm out}(\omega) = \mathcal{G}_S^\pm(\omega) c_\pm^e + \mathcal{G}_I^\pm(\omega) c_\mp^{e\dagger} + \sqrt{\frac{1-\eta^\pm}{\eta^\pm}}\left[(\mathcal{G}_S^\pm(\omega)+1) c_\pm^i + \mathcal{G}_I^\pm(\omega) c_\mp^{i\dagger}\right], \tag{11}$$

where we define the gain factors

$$\mathcal{G}_S^\pm(\omega) = \frac{\eta\kappa_\pm\left[\frac{\kappa_\mp}{2} - i(\omega + \Delta_\mp)\right]}{[i(\omega-\Delta_+) - \frac{\kappa_+}{2}][i(\omega+\Delta_-) - \frac{\kappa_-}{2}] - g^2} - 1,$$
$$\mathcal{G}_I^\pm(\omega) = \frac{-i\sqrt{\eta_-\eta_+}\kappa_\pm g e^{i\phi}}{[i(\omega-\Delta_+) - \frac{\kappa_+}{2}][i(\omega+\Delta_-) - \frac{\kappa_-}{2}] - g^2}, \tag{12}$$

where $|\mathcal{G}_I^\pm(\omega)|^2 = |\mathcal{G}_S^\pm(\omega)|^2 - 1$ for $\eta = 1$. The stability condition for the double-mode amplification can be extracted on the basis of the damping parameters of the initial (nonhybridized) modes, leading to $g < \kappa_a(1+\mathcal{C}_0)/2$, where $\mathcal{C}_0 = 4J^2/\kappa_a\kappa_b$ is the cooperatively of the interaction between the two resonators. In what follows, we report experimental investigations into both degenerate and nondegenerate amplification within a kinetic inductance superconducting resonator.

III. EXPERIMENTAL REALIZATION

The amplification process relies on the kinetic inductance exhibited by the superconducting film, which displays a nonlinear dependency on the applied current. This nonlinear behavior can be described by the

Ginzburg-Landau theory and the total inductance of the system [46,56–58] $L_k(I) = L_0[1 + (I/I^*)^2]$, where L_0 denotes the kinetic inductance of the film in the absence of current [54], while I^* is proportional to the critical current of the film and serves as a quantitative gauge of the film's responsiveness to the applied current I.

As shown in Fig. 2(a) and 2(b), at the core of this amplifier is a ring resonator, used as a nonlinear and dispersive mixing element. The fabrication process involves a straightforward single optical lithography step, as explained in Ref. [54]. The resonator is grounded and galvanically connected to both the pump line and the dc line. The generated or amplified signal is directed into a waveguide, which is coupled capacitively to the ring resonator. This design simplifies the measurement process and eliminates the requirement for a Bragg mirror or impedance-matching step coupler [34–38] within the system, resulting in a design that is exceptionally simple and compact. The mixing interaction between idler and signal modes is facilitated by the application of a direct current I_{dc}, modifying the circuit inductance

$$L_k(I) = L_0\left[1 + \left(\frac{I_{dc}}{I^*}\right)^2 + \frac{2I_{rf}I_{dc}}{I^{*2}} + \left(\frac{I_{rf}}{I^*}\right)^2\right], \quad (13)$$

where we consider $I = I_{dc} + I_{rf}$, in which I_{rf} is the current of the microwave signal. The first term in Eq. (13) gives the resonance frequency at zero current, whereas the second term characterizes a shift in the resonance frequency of the resonator due to the direct current, $\Delta\omega = -(\omega_0/2)\,(I_{dc}/I^*)^2$. The third term introduces the 3WM process, and the fourth term leads to Kerr nonlinearity [39]. The dependency of the resonance frequency of the mode on the current allows us to extract I^* and therefore infer the critical current of the superconducting sheet. Note that the ring resonator in our setup corresponds to resonator a as shown in Fig. 1, and it possesses a $\chi^{(2)}$ nonlinearity.

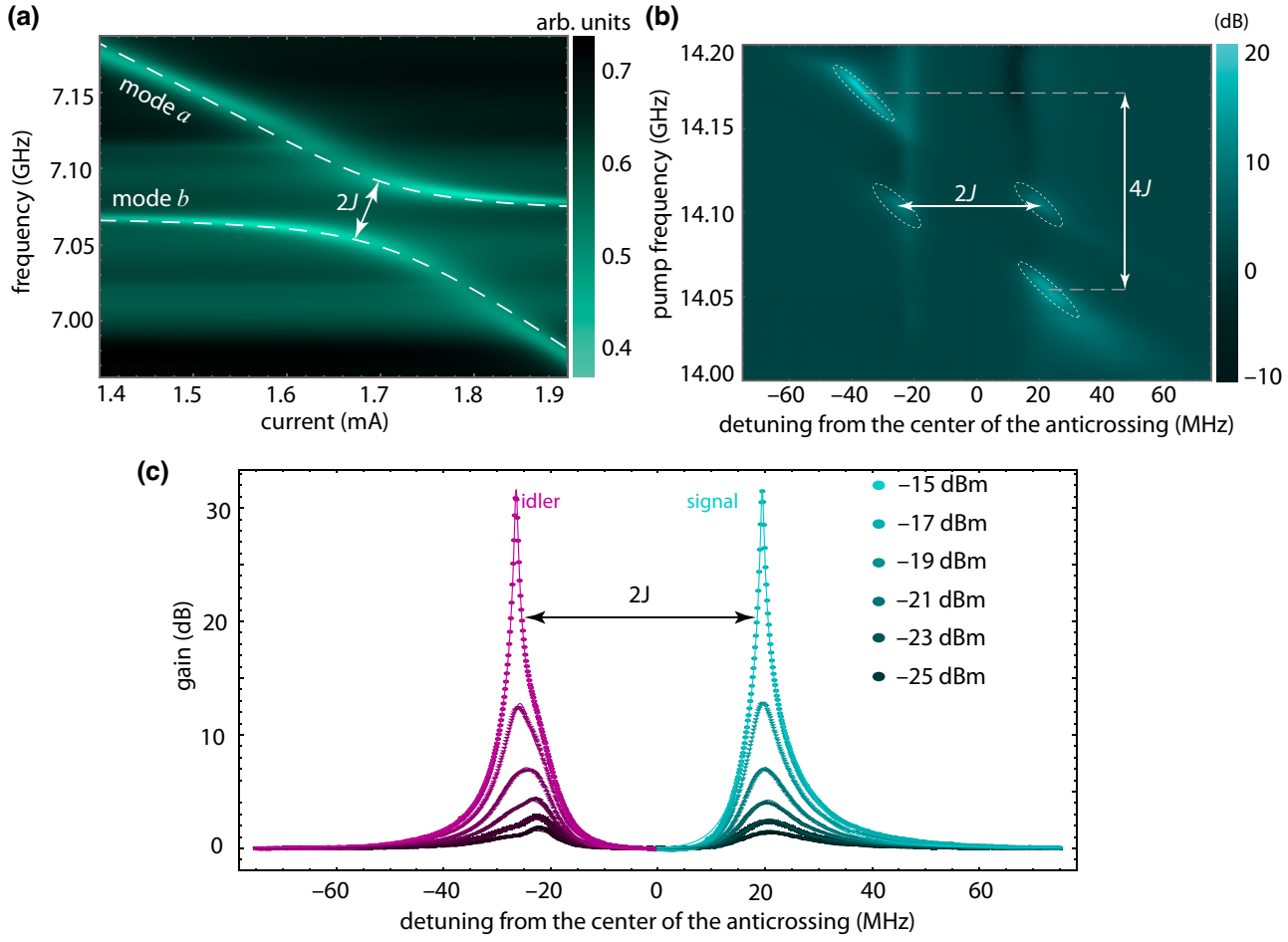

FIG. 3. (a) Appearance of the two modes and the anticrossing point as a function of the applied direct current. The two modes are separated by $2J \approx 43$ MHz. (b) Signal amplification versus pump frequency and detuning from the center of the anticrossing. (c) Phase-insensitive gain for the two modes at various pump powers versus the detuning from the center of the anticrossing.

In addition to the ring resonator, our system also has an auxiliary L-shaped resonator (corresponding to resonator b in Fig. 1), which is capacitively coupled to the ring resonator; see Fig. 2(b). The initial intent behind this setup was to have an additional transmission line for dual-sided probing and measuring of the ring resonator. However, this L-shaped section can also act as a resonator with a resonance mode ω_b close to that of the ring resonator, ω_a. As explained in Ref. [54], the behavior of the L-shaped resonator depends on the functionality of a cold switch directly connected to the resonator. When the switch is disconnected from the sample, the L-shaped resonator is essentially floating from both sides. Conversely, when the switch is connected to the sample, the L-shaped resonator is directly coupled to the input transmission line, effectively resulting in a resonator with a significantly large extrinsic coupling rate. Figure 2(c) shows the reflection response of the system when the cold switch is connected to the sample.

The large size of this auxiliary resonator minimizes its Kerr nonlinearity and allows the handling of substantial power without the critical current threshold being surpassed. Moreover, it can be directly wire-bonded, facilitating its use as a resonator with significant extrinsic coupling. This capability enables the measurement of the system from an alternative port. The auxiliary resonator is not connected to any dc wires, preventing the flow of biased current through it, thereby maintaining a constant resonance frequency. This setup provides a tunable nonlinear resonator (the ring resonator) connected to a nearby linear auxiliary resonator. This configuration accommodates a pair of coupled modes, initially separated by a spectral gap $\omega_a - \omega_b$ of approximately 360 MHz at zero bias current, as shown in Fig. 3(a). By application of a direct current, the frequency of the ring resonator can be adjusted, facilitating the alignment of the two modes at the anticrossing point with an intramode coupling strength J of approximately 21.5 MHz. As described in Sec. II, this coupling plays a critical role in selecting either single-mode amplification or double-mode amplification when the resonances reach the anticrossing point.

To initiate the 3WM process within the system, it is necessary to apply a bias current by using a stable and low-noise current source to supply the required current I_{dc}. Subsequently, at the millikelvin stage, this current is combined with the microwave pump, represented as I_p, through the use of a bias tee. Figure 2(c) visually demonstrates the influence of the direct current, showing that an increase in the current induces a downward shift in the frequency of the ring resonator that follows the expression $\Delta\omega = -(\omega_0/2)\,(I_{\mathrm{dc}}/I^*)^2$. By precisely knowing the applied current and fitting the frequency shift, we can deduce that $I^* = 5.86$ mA, a value consistent with a value previously measured for transmission lines of the same width [59] and critical currents of $I_c \lesssim 3.91$ mA [39]. Figure 2(d) shows the system's reflection from the probe port, demonstrating the resonance frequency of the ring resonator at $\omega_0/2\pi = 7.155$ GHz for $I_{\mathrm{dc}} = 1.575$ mA. Our fitting the resonator mode line shape provides $\kappa_{\mathrm{e}} = 19$ MHz and $\kappa_{\mathrm{i}} = 4$ MHz, leading to a waveguide-resonator coupling efficiency η of 0.82. The second mode is not immediately visible from Fig. 2(d). However, as described in Fig. 3(a), upon closer examination or by measuring with smaller steps, we can distinctly identify the anticrossing point and the existence of mode b.

IV. AMPLIFICATION

A. Single-mode amplification

To observe single-mode amplification we choose a bias current $I_{\mathrm{dc}} = 1.575$ mA far from the anticrossing point. As a result, we can effectively treat the system as being of single mode, and Hamiltonian (3) with $g = -I_{\mathrm{dc}} I_p \omega_0 / 4 I^{*2}$ [39] can fully describe the amplification process. In this case, the auxiliary resonator will not experience any amplification. We apply a strong pump at a frequency ω_p of approximately 14.29 GHz in addition to the bias current I_{dc}, which results in the down-conversion of pump photons, generating signal and idler photons at $\omega_p/2$. Figure 4(a) shows the nondegenerate gain profile as a function of detuning $\omega = \delta + (\omega_p/2)$ that is measured by our sweeping a coherent tone and capturing the maximum gain near half the pump frequency. We observe a substantial gain of approximately 43 dB, achieved with a pump power P_p of -23.8 dBm applied at the device's input. The gain profile is further analyzed with use of Eq. (5), resulting in $\kappa_{\mathrm{e}} = 28$ MHz, $\kappa_{\mathrm{i}} = 4$ MHz, and coupling efficiency $\eta = 0.9$. A comparison of coupling rates in the presence and in the absence of pump current shows an increase in the extrinsic coupling rate [39], which is attributed to kinetic inductance changes induced by the presence of the pump.

Additional amplification can be attained by one operating the KIPA in a degenerate mode, wherein both the signal and the idler have the same frequency, $\delta = 0$, and exhibit interference based on the phase difference $\Delta\phi$ between the pump and the probe. We use a weak probe signal at precisely half the pump frequency and measure the reflection of the system for various phases of the pump, as shown in Fig. 4(b). The collected data have been shifted to match $\Delta\phi = 0$, where we observe performance ranging from -30 dB of deamplification to in excess of 50 dB of amplification. Using Eq. (5), we once again fit the data, this time centered at $\omega = 0$. This analysis also provides insights into the extent of squeezing achievable, as during this operation, it becomes possible to squeeze vacuum fluctuations of one quadrature below the standard quantum limit [60].

Subsequently, we conduct an assessment of the KIPA's 1-dB compression point across various pump powers. This measurement serves to quantify the maximum input power the amplifier can accommodate before reaching saturation.

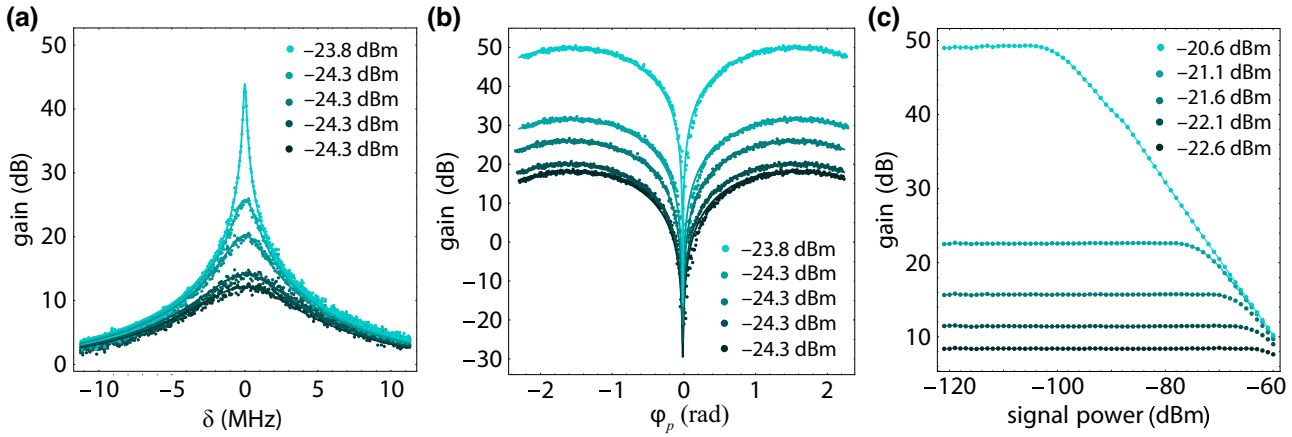

FIG. 4. (a) Single-mode phase-insensitive signal gain versus the frequency detuning from the resonator $\omega = \delta + (\omega_p/2)$ for different pump powers. The experimental results (dots) align well with the theoretical model (solid lines) outlined in the text. (b) Phase-sensitive gain as a function of the pump phase ϕ_p. A coherent tone positioned at $\delta = 0$ is measured while the pump phase is varied. The data are adjusted to align all dips at zero radians. The result is in good agreement with the theory. (c) The 1-dB compression point for a coherent tone at $\delta = 1$ kHz from the amplification center frequency. Power is varied to determine the 1-dB compression points at different pump powers.

Once again, we apply a probe signal and determine the point at which the KIPA experiences a 1-dB reduction in its maximum gain by increasing the probe power. The result shows a 1-dB compression power of approximately -73 dBm, corresponding to 20 dB of gain. This compression power is, on average, 3 orders of magnitude greater than that observed in Josephson junction–based amplifiers [47].

B. Double-mode amplification

As previously discussed, the amplifier design studied here accommodates two modes with an initial spectral separation of approximately 360 MHz at zero bias current. Nevertheless, by applying a direct current to the ring resonator, we can adjust the resonance frequency and shift it toward the anticrossing points. Note that the appearance of nonlinearity and, subsequently, amplification happens only in the ring resonator. This double-mode system can be effectively described with Eq. (1), where the nonlinear term $a^2 + a^{\dagger 2}$ is present only in the ring resonator due to the application of the bias current and mode b describes the auxiliary resonator (L-shaped resonator). Figure 3(a) shows how the ring resonator, mode a, evolves as the bias current is varied, eventually reaching the anticrossing point with the auxiliary resonator with mode b.

By our aligning the resonance of the two modes and holding them at the anticrossing point, which is achieved by our setting $I_{dc} = 1.68$ mA, the system can be operated within the nondegenerate (phase-insensitive) amplification regime described by Hamiltonian (10). Figure 3(b) shows the amplification versus the detuning from the anticrossing point and the pump frequency ω_p. Three distinct amplification regimes are evident in Fig, 3(b). In the initial region, when $\Delta \approx -J$, single-mode amplification is observed at $\omega_p \approx 14.059$ GHz, corresponding to the term c_-^2 in Hamiltonian (10). The second region indicates double-mode amplification or the activation of $c_- c_+$ terms at $\Delta \approx 0$, which is represented by the presence of two peaks at $\omega_p \approx 14.1$ GHz well separated by $2J$. In the third regime, amplification at $\omega_p \approx 14.15$ GHz occurs when $\Delta \approx J$, corresponding to the term c_+^2. Note that the pump-frequency separation between the first regime and the last regime, $\delta_p \approx 91$ MHz, is determined by the coupling strength between the two modes $\delta_p \approx 4J$, as anticipated. Figure 3(c) demonstrates double-mode (nondegenerate) amplification for different pump powers at $\Delta \approx 0$. It shows the amplification of the signal and idler modes, with up to 32 dB gain being achieved in both modes. The experimental results align well with our theoretical model for the coupled-mode system presented in Ref. [54].

V. NOISE CHARACTERIZATION AND EFFECT OF OPERATING TEMPERATURE

Another important aspect of a parametric amplifier is its noise behavior. We examine the noise performance of the KIPA in the single-mode regime by evaluating a chain of amplifiers and determining the additional noise introduced by the KIPA, as illustrated in Fig. 5(a). The output chain is divided into two parts: the KIPA, with gain G_k and input-referred added noise n_k, and the classical amplification chain, consisting of gain G_h and noise quanta n_h. This classical chain represents the collective gain and noise arising from the HEMT (near 4 K), the low-noise amplifier (at room temperature), and the cable losses across the chain. Near the nondegenerate amplification regime, the

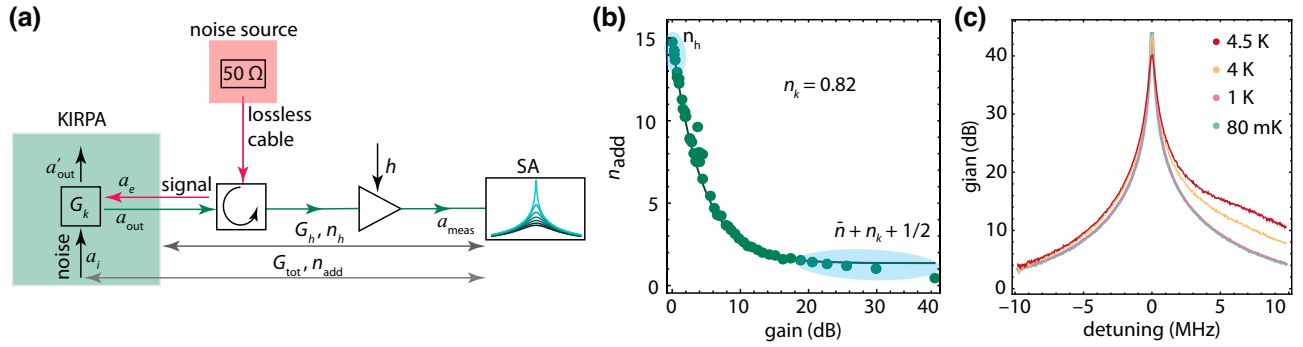

FIG. 5. (a) Noise-calibration setup. A 50-Ω terminator, varied in temperature, acts as the known noise source. The generated noise is directed to the KIPA at various gains. By using the Bose-Einstein distribution to fit the noise spectrum, we extract the total gain and noise quanta added by the amplification chain. (b) Noise quanta added by the whole amplification chain versus the gain of the KIPA when it is operating in the single-mode regime. At zero gain ($G_k = 0$), the noise of the classical amplification chain n_h dominates the added noise. In contrast, at large gains ($G_k \gg 1$), the noise added by the KIPA becomes noticeable $n_{add} \approx (\bar{n} + \frac{1}{2} + n_k)$. Our fitting the data using the theoretical model results in $n_k \approx 0.82$. (c) Comparison of the KIPA gain at different device temperatures (80 mK, 1 K, 4 K, and 4.5 K). Here, SA is spectrum analyzer.

field operator describing the entire chain is given by

$$a_{meas} = \sqrt{G_h} a_{out} + \sqrt{G_h - 1} h^\dagger, \tag{14}$$

where h represents the noise operator introduced by the classical amplification chain following the KIPA, while a_{out} characterizes the KIPA's output. By use of the above equation, the total noise quanta of the entire amplification chain can be computed (see Ref. [54] for further details):

$$N_{tot} \approx \hbar\omega G_{tot} \left[\frac{1}{2} \coth\left(\frac{\hbar\omega}{2k_B T} \right) + n_{add} \right], \tag{15}$$

where $G_{tot} = G_h G_k$ is the total gain, k_B is the Boltzmann constant, and

$$n_{add} = \frac{G_k - 1}{G_k} \left(\bar{n} + \frac{1}{2} + n_k \right) + \frac{n_h}{G_k} \tag{16}$$

is the total input-referred noise of the amplification chain, where $\bar{n}(T) = (e^{\hbar\omega/k_B T} - 1)^{-1}$ is the thermal noise at temperature T, and

$$n_k = 2 \left(\frac{1 - \eta}{\eta} \right) \left[\bar{n}(T_{dev}) + \frac{1}{2} \right], \tag{17}$$

is the input-referred noise added by the KIPA at a given device temperature T_{dev}. In the perfect-coupling regime $\eta \approx 1$, at a very low temperature $\bar{n} \approx 0$, and at large gain $G_k \gg 1$ such that $n_h/G_k \approx 0$, the total noise of the amplifier reduces to the vacuum noise $n_{add} \approx \frac{1}{2}$, as anticipated for an ideal nondegenerate quantum-limited amplifier.

By generating a known noise using a temperature-controlled 50-Ω-load noise source and feeding it into the KIPA, we estimate the overall device noise at various gains; see Fig. 5(a). First, during the noise calibration with the pump turned off, we deduce the gain G_h and added noise n_h of the classical amplification chain. Next, with the pump turned on, we measure the system's noise to determine G_k and n_{add} while the system operates in the single-mode-amplification regime, as shown in Fig. 5(b). In Fig. 5(b) for small KIPA gains ($G_k \approx 0$), the noise from the classical amplification chain becomes the main source of noise i.e., $n_{add} = n_h$. Conversely, at significantly high gains, the KIPA noise dominates the overall system noise $n_{add} \approx (\bar{n} + \frac{1}{2} + n_k)$. We use Eq. (16) to fit the experimental results, yielding $n_k \approx 0.82$ noise quanta. Part of the added noise comes from the rise in temperature of the mixing chamber of the dilution refrigerator, consequently increasing the sample's temperature to nearly 100 mK due to the application of direct current to the sample. This issue can be addressed by adjustment of the width of the sample and the use of thinner wires.

We additionally note that here we used the broadband variable-temperature stage method to calibrate the noise characteristics of our KIPA. One challenge associated with this approach is that the calibration tool used generates parasitic heat, which perturbs the mixing chamber of the dilution refrigerator and affects the effective temperature of the sample. Nonetheless, in Supplemental Material [54], we introduce an alternative approach to calibrate the sample noise. Other approaches, such as the use of shot-noise tunnel junctions, offer a potential avenue for more-thorough validation of the noise added by the amplifier [61].

As a final remark, we describe the operational performance of our device at different temperatures. The kinetic inductance properties of the KIPA and its independence from Josephson junctions offer a substantial advantage when it comes to our operating it at higher temperatures [62], a limitation that affects JPA and JTWPA devices.

We can test and operate the amplifier at different temperatures and measure the gain at different phases of the process. In Fig. 5(c), the gain of the amplifier in the single mode is illustrated at various device temperatures. It is apparent that the amplifier effectively maintains its gain performance, even at temperatures reaching up to 4.5 K. However, because of technical limitations and the inability to regulate the dilution refrigerator's temperature beyond 4.5 K, evaluation of the device's performance at higher temperatures was unattainable.

VI. CONCLUSION AND DISCUSSION

In summary, we have developed a junction-free quantum-limited amplifier based on kinetic inductance superconductivity. The design of our amplifier is inherently simple and does not necessitate complex circuitry or impedance-matching step couplers for amplification generation [39]. Overcoming the limitations of conventional Josephson-junction amplifiers, this device operates at temperatures above 4.5 K. Its double-mode capability and tunability through bias current facilitates selective operation in both the single-mode-amplification regime and the double-mode-amplification regime, achieving gains surpassing 50 dB in the single-mode configuration and 32 dB in the double-mode configuration, while adding only 0.82 noise quanta. Compared with Josephson junction–based amplifiers, our device presents a remarkably improved 1-dB compression point of −73 dB at 20-dB gain mainly due to the small contribution of the self-Kerr-term in the system. However, even though we did not measure the magnetic field dependency, high-kinetic-inductance Nb-Ti-N resonators demonstrate exceptional magnetic field compatibility, with fields up to 6 T [48]. Moreover, recent studies affirm the maintenance of amplification performance up to 1 T [40,42,63].

This amplifier can potentially be used in a broad range of quantum applications, particularly in the domain of quantum computing. Its adaptability and resilience make it a fitting candidate for integration into future superconducting quantum computers, enhancing microwave measurements and enabling fast and accurate readout of superconducting qubits and spins. Additionally, its ability to perform effectively at higher temperatures suggests its utility in quantum sensing and reading applications, such as quantum illumination and radar [30]. Moreover, its resilience to magnetic fields opens possibilities for integration into hybrid quantum circuits or for the readout of spins and color centers that necessitate magnetic fields for their control.

The low loss of our device enables the generation of nonclassical radiation, such as entanglement and squeezing within the circuit. Quantum entanglement finds applications in quantum sensing, linking remote quantum nodes, and establishing entangled clusters across a chip. Squeezing, however, is a valuable resource for universal quantum computing [64,65]. The simple design, high fabrication yield, low loss, and scalability of our device could potentially find applications in microwave continuous-variable quantum computing [66].

ACKNOWLEDGMENTS

We thank Joe Salfi, Leonid Belostotski, and Mohammad Khalifa helpful comments and discussions. S.B. acknowledges funding by the Natural Sciences and Engineering Research Council of Canada through its Discovery Grant and Quantum Alliance Grant, funding and advisory support provided by Alberta Innovates through the Accelerating Innovations into CarE (AICE)—Concepts program, support from Alberta Innovates and the Natural Sciences and Engineering Research Council of Canada through the Advance Grant project, and Alliance Quantum Consortium. This project is funded (in part) by the Government of Canada.

[1] C. M. Caves, Quantum limits on noise in linear amplifiers, Phys. Rev. D **26**, 1817 (1982).
[2] A. A. Clerk, M. H. Devoret, S. M. Girvin, F. Marquardt, and R. J. Schoelkopf, Introduction to quantum noise, measurement, and amplification, Rev. Mod. Phys. **82**, 1155 (2010).
[3] J. Aumentado, Superconducting parametric amplifiers: The state of the art in Josephson parametric amplifiers, IEEE Microw. Mag. **21**, 45 (2020).
[4] A. Blais, A. L. Grimsmo, S. M. Girvin, and A. Wallraff, Circuit quantum electrodynamics, Rev. Mod. Phys. **93**, 025005 (2021).
[5] M. A. Castellanos-Beltran and K. W. Lehnert, Widely tunable parametric amplifier based on a superconducting quantum interference device array resonator, Appl. Phys. Lett. **91**, 083509 (2007).
[6] M. Hatridge, R. Vijay, D. H. Slichter, J. Clarke, and I. Siddiqi, Dispersive magnetometry with a quantum limited SQUID parametric amplifier, Phys. Rev. B **83**, 134501 (2011).
[7] N. Bergeal, F. Schackert, M. Metcalfe, R. Vijay, V. E. Manucharyan, L. Frunzio, D. E. Prober, R. J. Schoelkopf, S. M. Girvin, and M. H. Devoret, Phase-preserving amplification near the quantum limit with a Josephson ring modulator, Nature **465**, 64 (2010).
[8] C. Macklin, K. O'Brien, D. Hover, M. E. Schwartz, V. Bolkhovsky, X. Zhang, W. D. Oliver, and I. Siddiqi, A near–quantum-limited Josephson traveling-wave parametric amplifier, Science **350**, 307 (2015).
[9] M. Esposito, A. Ranadive, L. Planat, and N. Roch, Perspective on traveling wave microwave parametric amplifiers, Appl. Phys. Lett. **119**, 120501 (2021).
[10] T. Walter, P. Kurpiers, S. Gasparinetti, P. Magnard, A. Potočnik, Y. Salathé, M. Pechal, M. Mondal, M. Oppliger,

C. Eichler, and A. Wallraff, Rapid high-fidelity single-shot dispersive readout of superconducting qubits, Phys. Rev. Appl. **7**, 054020 (2017).

[11] J. Heinsoo, C. K. Andersen, A. Remm, S. Krinner, T. Walter, Y. Salathé, S. Gasparinetti, J.-C. Besse, A. Potočnik, A. Wallraff, and C. Eichler, Rapid high-fidelity multiplexed readout of superconducting qubits, Phys. Rev. Appl. **10**, 034040 (2018).

[12] R. Vijay, D. H. Slichter, and I. Siddiqi, Observation of quantum jumps in a superconducting artificial atom, Phys. Rev. Lett. **106**, 110502 (2011).

[13] E. Jeffrey, D. Sank, J. Y. Mutus, T. C. White, J. Kelly, R. Barends, Y. Chen, Z. Chen, B. Chiaro, A. Dunsworth, A. Megrant, P. J. J. O'Malley, C. Neill, P. Roushan, A. Vainsencher, J. Wenner, A. N. Cleland, and J. M. Martinis, Fast accurate state measurement with superconducting qubits, Phys. Rev. Lett. **112**, 190504 (2014).

[14] W. Vine, M. Savytskyi, A. Vaartjes, A. Kringhøj, D. Parker, J. Slack-Smith, T. Schenkel, K. Mølmer, J. C. McCallum, B. C. Johnson, A. Morello, and J. J. Pla, In situ amplification of spin echoes within a kinetic inductance parametric amplifier, Sci. Adv. **9**, eadg1593 (2023).

[15] S. Schaal, I. Ahmed, J. A. Haigh, L. Hutin, B. Bertrand, S. Barraud, M. Vinet, C.-M. Lee, N. Stelmashenko, J. W. A. Robinson, J. Y. Qiu, S. Hacohen-Gourgy, I. Siddiqi, M. F. Gonzalez-Zalba, and J. J. L. Morton, Fast gate-based readout of silicon quantum dots using Josephson parametric amplification, Phys. Rev. Lett. **124**, 067701 (2020).

[16] J. Stehlik, Y.-Y. Liu, C. M. Quintana, C. Eichler, T. R. Hartke, and J. R. Petta, Fast charge sensing of a cavity-coupled double quantum dot using a Josephson parametric amplifier, Phys. Rev. Appl. **4**, 014018 (2015).

[17] J. Kerckhoff, R. W. Andrews, H. S. Ku, W. F. Kindel, K. Cicak, R. W. Simmonds, and K. W. Lehnert, Tunable coupling to a mechanical oscillator circuit using a coherent feedback network, Phys. Rev. X **3**, 021013 (2013).

[18] M. A. Castellanos-Beltran, K. D. Irwin, G. C. Hilton, L. R. Vale, and K. W. Lehnert, Amplification and squeezing of quantum noise with a tunable Josephson metamaterial, Nat. Phys. **4**, 929 (2008).

[19] K. G. Fedorov, L. Zhong, S. Pogorzalek, P. Eder, M. Fischer, J. Goetz, E. Xie, F. Wulschner, K. Inomata, T. Yamamoto, Y. Nakamura, R. Di Candia, U. Las Heras, M. Sanz, E. Solano, E. P. Menzel, F. Deppe, A. Marx, and R. Gross, Displacement of propagating squeezed microwave states, Phys. Rev. Lett. **117**, 020502 (2016).

[20] F. Mallet, M. A. Castellanos-Beltran, H. S. Ku, S. Glancy, E. Knill, K. D. Irwin, G. C. Hilton, L. R. Vale, and K. W. Lehnert, Quantum state tomography of an itinerant squeezed microwave field, Phys. Rev. Lett. **106**, 220502 (2011).

[21] K. W. Murch, S. J. Weber, C. Macklin, and I. Siddiqi, Observing single quantum trajectories of a superconducting quantum bit, Nature **502**, 211 (2013).

[22] S. J. Weber, A. Chantasri, J. Dressel, A. N. Jordan, K. W. Murch, and I. Siddiqi, Mapping the optimal route between two quantum states, Nature **511**, 570 (2014).

[23] A. Caldwell, G. Dvali, B. Majorovits, A. Millar, G. Raffelt, J. Redondo, O. Reimann, F. Simon, and F. Steffen, (MADMAX Working Group), Dielectric haloscopes: A new way to detect axion dark matter, Phys. Rev. Lett. **118**, 091801 (2017).

[24] J. Jeong, S. Youn, S. Bae, J. Kim, T. Seong, J. E. Kim, and Y. K. Semertzidis, Search for invisible axion dark matter with a multiple-cell haloscope, Phys. Rev. Lett. **125**, 221302 (2020).

[25] K. Wurtz, B. Brubaker, Y. Jiang, E. Ruddy, D. Palken, and K. Lehnert, Cavity entanglement and state swapping to accelerate the search for axion dark matter, PRX Quantum **2**, 040350 (2021).

[26] K. M. Backes *et al.* A quantum enhanced search for dark matter axions, Nature **590**, 238 (2021).

[27] S. Barzanjeh, S. Guha, C. Weedbrook, D. Vitali, J. H. Shapiro, and S. Pirandola, Microwave quantum illumination, Phys. Rev. Lett. **114**, 080503 (2015).

[28] S. Barzanjeh, S. Pirandola, D. Vitali, and J. M. Fink, Microwave quantum illumination using a digital receiver, Sci. Adv. **6**, eabb0451 (2020).

[29] R. Assouly, R. Dassonneville, T. Peronnin, A. Bienfait, and B. Huard, Quantum advantage in microwave quantum radar, Nat. Phys. **19**, 1418 (2023).

[30] R. G. Torrome and S. Barzanjeh, Advances in quantum radar and quantum lidar, Prog. Quantum Electron. **93**, 100497 (2024).

[31] B. Yurke, L. R. Corruccini, P. G. Kaminsky, L. W. Rupp, A. D. Smith, A. H. Silver, R. W. Simon, and E. A. Whittaker, Observation of parametric amplification and deamplification in a Josephson parametric amplifier, Phys. Rev. A **39**, 2519 (1989).

[32] M. Renger, S. Pogorzalek, Q. Chen, Y. Nojiri, K. Inomata, Y. Nakamura, M. Partanen, A. Marx, R. Gross, F. Deppe, and K. G. Fedorov, Beyond the standard quantum limit for parametric amplification of broadband signals, npj Quantum Inf. **7**, 160 (2021).

[33] L. Planat, R. Dassonneville, J. P. Martínez, F. Foroughi, O. Buisson, W. Hasch-Guichard, C. Naud, R. Vijay, K. Murch, and N. Roch, Understanding the saturation power of Josephson parametric amplifiers made from squid arrays, Phys. Rev. Appl. **11**, 034014 (2019).

[34] E. A. Tholén, A. Ergül, K. Stannigel, C. Hutter, and D. B. Haviland, Parametric amplification with weak-link nonlinearity in superconducting microresonators, Phys. Scr. **2009**, 014019 (2009).

[35] B. Ho Eom, P. K. Day, H. G. LeDuc, and J. Zmuidzinas, A wideband, low-noise superconducting amplifier with high dynamic range, Nat. Phys. **8**, 623 (2012).

[36] S. Chaudhuri, D. Li, K. D. Irwin, C. Bockstiegel, J. Hubmayr, J. N. Ullom, M. R. Vissers, and J. Gao, Broadband parametric amplifiers based on nonlinear kinetic inductance artificial transmission lines, Appl. Phys. Lett. **110**, 152601 (2017).

[37] A. Anferov, A. Suleymanzade, A. Oriani, J. Simon, and D. I. Schuster, Millimeter-wave four-wave mixing via kinetic inductance for quantum devices, Phys. Rev. Appl. **13**, 024056 (2020).

[38] M. Malnou, M. Vissers, J. Wheeler, J. Aumentado, J. Hubmayr, J. Ullom, and J. Gao, Three-wave mixing kinetic

inductance traveling-wave amplifier with near-quantum-limited noise performance, PRX Quantum **2**, 010302 (2021).
[39] D. J. Parker, M. Savytskyi, W. Vine, A. Laucht, T. Duty, A. Morello, A. L. Grimsmo, and J. J. Pla, Degenerate parametric amplification via three-wave mixing using kinetic inductance, Phys. Rev. Appl. **17**, 034064 (2022).
[40] S. Frasca, C. Roy, G. Beaulieu, and P. Scarlino, Three-wave-mixing quantum-limited kinetic inductance parametric amplifier operating at 6 T near 1 K, Phys. Rev. Appl. **21**, 024011 (2024).
[41] M. Xu, R. Cheng, Y. Wu, G. Liu, and H. X. Tang, Magnetic field-resilient quantum-limited parametric amplifier, PRX Quantum **4**, 010322 (2023).
[42] M. Khalifa and J. Salfi, Nonlinearity and parametric amplification of superconducting nanowire resonators in magnetic field, Phys. Rev. Appl. **19**, 034024 (2023).
[43] L. Zhong, E. P. Menzel, R. D. Candia, P. Eder, M. Ihmig, A. Baust, M. Haeberlein, E. Hoffmann, K. Inomata, T. Yamamoto, Y. Nakamura, E. Solano, F. Deppe, A. Marx, and R. Gross, Squeezing with a flux-driven Josephson parametric amplifier, New J. Phys. **15**, 125013 (2013).
[44] S. Barzanjeh, E. S. Redchenko, M. Peruzzo, M. Wulf, D. P. Lewis, G. Arnold, and J. M. Fink, Stationary entangled radiation from micromechanical motion, Nature **570**, 480 (2019).
[45] M. Esposito, A. Ranadive, L. Planat, S. Leger, D. Fraudet, V. Jouanny, O. Buisson, W. Guichard, C. Naud, J. Aumentado, F. Lecocq, and N. Roch, Observation of two-mode squeezing in a traveling wave parametric amplifier, Phys. Rev. Lett. **128**, 153603 (2022).
[46] A. J. Annunziata, D. F. Santavicca, L. Frunzio, G. Catelani, M. J. Rooks, A. Frydman, and D. E. Prober, Tunable superconducting nanoinductors, Nanotechnology **21**, 445202 (2010).
[47] M. Esposito, A. Ranadive, L. Planat, and N. Roch, Perspective on traveling wave microwave parametric amplifiers, Appl. Phys. Lett. **119**, 120501 (2021).
[48] N. Samkharadze, A. Bruno, P. Scarlino, G. Zheng, D. P. DiVincenzo, L. DiCarlo, and L. M. K. Vandersypen, High-kinetic-inductance superconducting nanowire resonators for circuit QED in a magnetic field, Phys. Rev. Appl. **5**, 044004 (2016).
[49] L. Zhang, W. Peng, L. X. You, and Z. Wang, Superconducting properties and chemical composition of NbTiN thin films with different thickness, Appl. Phys. Lett. **107**, 122603 (2015).
[50] P. Winkel, I. Takmakov, D. Rieger, L. Planat, W. Hasch-Guichard, L. Grünhaupt, N. Maleeva, F. Foroughi, F. Henriques, K. Borisov, J. Ferrero, A. V. Ustinov, W. Wernsdorfer, N. Roch, and I. M. Pop, Nondegenerate parametric amplifiers based on dispersion-engineered Josephson-junction arrays, Phys. Rev. Appl. **13**, 024015 (2020).
[51] V. V. Sivak, S. Shankar, G. Liu, J. Aumentado, and M. H. Devoret, Josephson array-mode parametric amplifier, Phys. Rev. Appl. **13**, 024014 (2020).
[52] C. Eichler, Y. Salathe, J. Mlynek, S. Schmidt, and A. Wallraff, Quantum-limited amplification and entanglement in coupled nonlinear resonators, Phys. Rev. Lett. **113**, 110502 (2014).
[53] S. Boutin, D. M. Toyli, A. V. Venkatramani, A. W. Eddins, I. Siddiqi, and A. Blais, Effect of higher-order nonlinearities on amplification and squeezing in Josephson parametric amplifiers, Phys. Rev. Appl. **8**, 054030 (2017).
[54] See Supplemental Material at http://link.aps.org/supplemental/10.1103/PhysRevApplied.21.064052 for additional information on the measurement setup, sample fabrication and packaging, noise calibration, and full theoretical modeling of the system.
[55] B. A. Levitan, A. Metelmann, and A. A. Clerk, Optomechanics with two-phonon driving, New J. Phys. **18**, 093014 (2016).
[56] A. B. Pippard and W. L. Bragg, Field variation of the superconducting penetration depth, Proc. R. Soc. Lond. A. Math. Phys. Sci. **203**, 210 (1950).
[57] A. B. Pippard and W. L. Bragg, An experimental and theoretical study of the relation between magnetic field and current in a superconductor, Proc. R. Soc. Lond. A Math. Phys. Sci. **216**, 547 (1953).
[58] J. Zmuidzinas, Superconducting microresonators: Physics and applications, Ann. Rev. Condens. Matter Phys. **3**, 169 (2012).
[59] H. L. Hortensius, E. F. C. Driessen, T. M. Klapwijk, K. K. Berggren, and J. R. Clem, Critical-current reduction in thin superconducting wires due to current crowding, Appl. Phys. Lett. **100**, 182602 (2012).
[60] R. E. Slusher, L. W. Hollberg, B. Yurke, J. C. Mertz, and J. F. Valley, Observation of squeezed states generated by four-wave mixing in an optical cavity, Phys. Rev. Lett. **55**, 2409 (1985).
[61] M. Malnou, T. F. Q. Larson, J. D. Teufel, F. Lecocq, and J. Aumentado, Low-noise cryogenic microwave amplifier characterization with a calibrated noise source, arXiv:2312.14900 (2023).
[62] M. Malnou, J. Aumentado, M. Vissers, J. Wheeler, J. Hubmayr, J. Ullom, and J. Gao, Performance of a kinetic inductance traveling-wave parametric amplifier at 4 kelvin: Toward an alternative to semiconductor amplifiers, Phys. Rev. Appl. **17**, 044009 (2022).
[63] A. Vaartjes, A. Kringhøj, W. Vine, T. Day, A. Morello, and J. J. Pla, Strong microwave squeezing above 1 tesla and 1 kelvin, Nat. Commun. **15**, 4229 (2024).
[64] N. C. Menicucci, P. van Loock, M. Gu, C. Weedbrook, T. C. Ralph, and M. A. Nielsen, Universal quantum computation with continuous-variable cluster states, Phys. Rev. Lett. **97**, 110501 (2006).
[65] N. C. Menicucci, Fault-tolerant measurement-based quantum computing with continuous-variable cluster states, Phys. Rev. Lett. **112**, 120504 (2014).
[66] L. S. Madsen, F. Laudenbach, M. F. Askarani, F. Rortais, T. Vincent, J. F. F. Bulmer, F. M. Miatto, L. Neuhaus, L. G. Helt, M. J. Collins, A. E. Lita, T. Gerrits, S. W. Nam, V. D. Vaidya, M. Menotti, I. Dhand, Z. Vernon, N. Quesada, and J. Lavoie, Quantum computational advantage with a programmable photonic processor, Nature **606**, 75 (2022).